Measurements of Equivalence Ratio Fluctuations in a Lean Premixed Prevaporized (LPP) Combustor and its Correlation to Combustion Instability

Quang-Viet Nguyen
National Aeronautics and Space Administration
Glenn Research Center
Cleveland, OH 44135

Abstract:
Experimental evidence correlating equivalence ratio fluctuations with combustion instabilities and NO_X emissions in a jet-A fueled lean premixed prevaporized (LPP) combustor is presented. Real-time laser absorption measurements of equivalence ratio, together with dynamic combustor pressure, flame luminosity and fuel pressure were obtained at inlet air conditions up 16.7 atm and 817 K. Time and frequency space analysis revealed high levels of acoustic coupling between all measured variables. Equivalence ratio and dynamic pressure cross-correlations were found to predict the level of combustion instability. Furthermore, NO_X production was found to follow the RMS flame luminosity and RMS combustor pressure. However, the unmixedness parameter was not found to predict NO_X production in this system. The fuel premixer advection time was found to have a significant and direct effect on the level of combustion instability.

Introduction:

Stationary gas turbine engines have benefited greatly from the many advances in lean premixed (LP) combustion technologies developed over the past decade; sub 25 ppmv NO_X emissions levels (corrected to 15% O_2) are now routine, and sub 10 ppmv NO_X levels are currently being pursued [1]. Low NO_X operation of a LP gas turbine combustor is realized by burning the fuel-air mixture at a fuel-lean equivalence ratio (Phi) such that combustion temperatures are kept below 1700 K, thereby preventing the formation of thermal NO, the principal component of NO_X [2]. However, variations in the uniformity of the fuel-air mixture in both space [3] and time [4], have a strong effect on the low NO_X emissions performance of LP combustion systems. Low NO_X operation using LP combustion also has the potential problems of high levels of unburned hydrocarbons (UHC) and carbon monoxide (CO) emissions resulting from the increased levels of combustion instability and localized flame extinction [2, 5]. The role of the premixer in LP combustion systems cannot be understated: bad premixers produce more NO_X , UHC, and CO emissions than good premixers [6]. The term 'good' refers to the extent of fuel-air mixture uniformity in space and time. An ideal premixer has a single-valued output fuel-air mixture distribution. In order to quantify fuel-air mixture uniformity, a non-dimensional unmixedness parameter is often used. The unmixedness parameter ranges from 0 for perfectly mixed mixtures, to 1 for a mixture with maximum variance [4]. Mixture uniformity can also be quantified by a probability density function (PDF) of the fuel-air mixture (or equivalence ratio). The PDF of Phi is a histogram that shows how much 'time' a particular injector spends at a given equivalence ratio. An ideal injector would have a delta function at a specified Phi for a PDF.

The application of LP combustion to stationary and automotive gas turbine engines has been investigated by Anderson [7]. The extension of this work to advanced low emissions aeroengine applications for the reduction of stratospheric cruise emissions was described by Mularz [8] and investigated later by Lyons [3]. For aircraft use, LP combustion requires liquid kerosene based fuels such as jet-A rather than gaseous fuels typically used by stationary LP combustion turbine engines. Hence the term Lean-Premixed Prevaporized (LPP) combustion is used delineate liquid-fueled LP combustion from gaseous-fueled LP combustion. Since low-NO_X operation of LP/LPP combustion systems requires that the equivalence ratio to be kept very close to the lean stability limit, the threat of combustion induced instabilities manifested as large dynamic pressure fluctuations in the combustor is a constant threat. To further exacerbate the problem of combustion instability, LP/LPP combustion systems are inherently more prone to acoustic oscillations due to the fact that a homogeneous mixture of fuel-air, such as that exists in LP/LPP combustors, can amplify acoustic perturbations much more efficiently than conventional non-premixed combustion systems, and LP/LPP combustors have less acoustic damping due to their hard-wall combustion chambers [9]. The amplification of an acoustic pressure wave by a LP flame is explained through the Rayleigh criterion, which states that if the rate of heat release in a combustor is in phase with the pressure, a feedback mechanism will exist that amplifies the acoustic perturbations [10]. The problem of acoustic instabilities is formidable as the high pressure oscillations can substantially degrade mechanical component lifetimes in an engine, and at worst, can literally shake an engine apart. Such problems are of course, unacceptable in an aircraft engine where reliability is paramount.

Due to the importance of combustion instabilities in gas turbine engines, many studies have addressed the issue of modeling and controlling combustion instabilities in LP combustion: Bloxsidge et al [11] examined the active control of reheat buzz in a combustor; Darling et al [12] presented measurements of combustion noise at high pressures in a LPP combustor; Lieuwen and Zin [13] presented a theoretical model describing the role of equivalence ratio fluctuations in LP combustor instabilities; Richards and Janus [9] characterized combustion instabilities in a LP combustor and correlated it with the concept of injector time lag; Paxson [14] modeled combustion instabilities in a LPP combustor using a sectored-1-dimensional code; Cohen et al [15] developed an experimental test stand that could replicate the instabilities in a real aeroengine; Johnson et al [16] and Sattinger et al [17] demonstrated the suppression of combustion instabilities using active control methods; and Steele et al [1] demonstrated a passive combustion instability control technique for LP combustors. These studies have proposed several mechanisms that explain the causes of acoustic instabilities in LP combustion systems. They all basically involve the concept of a perturbation to the rate of heat release which amplifies a pressure oscillation in the combustion chamber if the Rayleigh criterion is satisfied. In particular, the fluctuations in the equivalence ratio (Phi) of the lean premixed fuel-air mixture is thought to play a key role in the stability of a LP combustor [9, 13]. Lieuwen and Zin [13] indicated that there is a need for direct measurements of the fluctuating equivalence ratio in LP combustors for the purposes of validating their combustion instability model.

Since direct measurements of heat-release in a gas turbine combustor are not possible or practical, techniques to measure the rate of heat release indirectly through bulk flame luminosity [11], chemiluminescence of OH^* [9], LIF measurements of fuel concentration [18], extractive suction probe laser absorption measurements of air-fuel ratios [19, 20], and in situ laser absorption measurements [21], have been performed to measure the rate of heat release indirectly. This work extends the technique used by Nguyen et al [21] in a high pressure LPP combustor by including dynamic measurements of combustor and fuel line pressure, flame luminosity and extractively sampled gaseous emissions using a 'generic' (non-proprietary) LPP fuel injector for the purposes of providing combustion instability data that can be modeled using the current theories of combustion instabilities.

Measurement Theory:

The absorption of light by the C-H vibrational stretching mode near 2900 cm^{-1} permits the use of the 3.39 μm HeNe laser for the sensitive detection of most HC molecules [22]. The absorption obeys the Beer-Lambert law and is quantitative in nature, provided the absorption coefficient, the pathlength, temperature and pressure are known. If the presence of liquid fuel droplets causes attenuation in the

Submitted to *J. of Engr. for Gas Turbines and Power* May 14, 2001.

transmitted optical intensity, then a second non-spectrally absorbing wavelength can be used to correct for the effects of the droplet scattering and absorption of the IR light. Drallmeier [23] derived an expression using Mie scattering theory that permits the effects of droplet scattering to be accounted for (for droplets above 20 μm) in diameter. When the bulk of droplets causing attenuation are below 20 μm in diameter, the error in the correction becomes progressively worse. The time varying mole fraction (c) of the fuel air mixture (assuming no combustion) is given by:

$$\chi(t) = \frac{-\log(\tau_{VIS}\,\eta - \tau_{IR})\,R\,T}{\varepsilon\,L\,P_{TOTAL}} \qquad (1)$$

where the optical transmission at the infrared and visible wavelengths are given by t_{IR} and t_{VIS}, respectively, R is the universal gas constant, T is the temperature, L is the pathlength, P is the total pressure, h is the optical thickness ratio, and e is the decadic extinction coefficient. The decadic extinction coefficient is an absorption coefficient cast in terms of the base 10 logarithm and has been measured for many HC molecules by Tsuboi et al [22] and has units of [cm^2 mol^{-1}]. The optical thickness ratio is approximately 1.1 for 3.39 μm wavelength light used with a 633 nm wavelength light for the non-spectrally absorbing reference beam [23].

For measurements located in a region where combustion has not taken place, the temperature of the gases is known from the inlet conditions to the combustor, furthermore, the assumption that the balance of the of the gases is composed of air. This permits converting the measurement of the mole fraction of the fuel vapor to a measurement of the equivalence ratio. The decadic extinction coefficient for kerosene type jet fuels has not been measured over an extensive range of temperatures and pressures. However, the effect of pressure and temperature variations can be approximated using relations by Yoshiyama et al [24] and Fuss et al [25], respectively. The decadic extinction coefficient for jet-A is assumed to scale with $P^{-0.302}$ as suggested by Yoshiyama et al [24] for methane. For the high temperatures encountered in this study, the jet-A compounds are assumed to be thermally cracked and decomposed into smaller paraffin-like HC's whose integrated spectral band intensity near 3.4 μm scales with temperature according to ($1/T$) as measured by Fuss at al [25]. In order to measure the decadic extinction coefficient of jet-A, several high temperature measurements are performed and the assumption that all the liquid jet fuel is evaporated and exists only in the gas phase is made. By averaging several of these measurements, a base decadic extinction coefficient is determined. This coefficient is then scaled by the nominal operating temperature and pressure according to the above relations for use at different temperatures and pressures. The following expression was used for the decadic extinction coefficient of jet-A over the conditions encountered in this study.

$$e = 5.30 \times 10^4\,(805\ \mathrm{K}/T)\,(P/10.0\ \mathrm{atm})^{-0.302}\ [\mathrm{cm^2\ mol^{-1}}]\,. \qquad (2)$$

The decadic extinction coefficient generated by this expressions is within the typical range of values for typical HC's measured by Tsuboi et al [22]. However, the composition of jet-A varies greatly between production batches, locality, etc. Thus, this expression is only approximate and an in-situ calibration such as performed for this study should be performed for future studies to ensure the best accuracy.

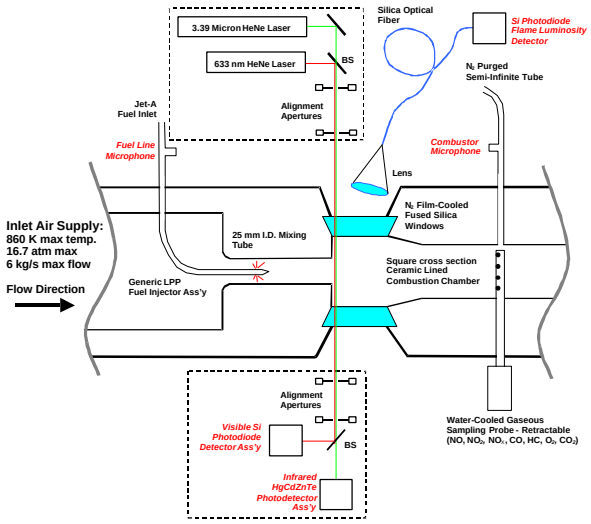

Figure 1: Schematic of the infrared absorption optical setup as installed in the CE-5B-2 flame tube facility at NASA Glenn Research Center. Real-time data instrumentation in the figure is denoted by italics. The combustion chamber microphone port and extractive gaseous sampling probe are located 38 cm downstream of the combustor dome face. A purged, semi-infinite 'T' arrangement for the microphones was used to improve acoustic fidelity. A water quench spray is located 84 cm downstream from the combustor dome face (not shown). A 4-port area-averaged water-cooled suction probe collects the gaseous emissions sample and a heated line transfers the gases to a suite of gas-bench analyzers.

Experimental:

Figure 1 shows a schematic of the experimental arrangement located in the CE-5B test facility at NASA GRC. This optically accessible high-pressure combustion rig is described in detail elsewhere [26, 27]. The optical absorption setup is similar to that described by Nguyen et al [21] with some improvements and also with the addition of dynamic combustion and fuel pressure transducers and a fiber optically coupled flame luminosity detector. The infrared absorption setup used a polarized 2 mW 3.39 μm HeNe laser coaxially superimposed onto a 10 mW 633 nm HeNe laser through a dichroic Si beamsplitter. The beams were directed through two circular apertures defining the optic axis using mirrors. The combined beams were directed through a 12.5 mm thick UV grade fused silica window (80% transmission at 3.4 μm) located on the high pressure test rig and across the measurement zone located approximately 5 mm downstream from the combustor dome face. The transmitted beam exits the high pressure rig through another identical UV grade fused silica window and is aligned with the receiver unit. The optical receiver unit consists of a pair of adjustable apertures to aid alignment and to reduce stray background light interferences, another Si dichroic beamsplitter, and visible and infrared detector units. The infrared portion of the beam is focused to overfill a 0.5mm x 0.5mm optically immersed HgCdZnTe, room-temperature, photo-voltaic detector/preamplifier using a 25 mm focal length UV grade fused silica lens. The visible portion of the transmitted beam is directed at a light-integrating device to reduce the effect of beam steering on the visible signal. The light integrating device consisted of an opal glass diffuser mounted on a diffuse white chamber to which an amplified Si photodiode detector was mounted. The 633 nm light falling on the opal glass diffuser generated a signal that was relatively independent of the position of the beam on the opal glass screen. This reduces the effects of thermal gradient beam steering inside the combustor which would be manifested as small displacements of the visible beam spot on the opal glass screen. Thus, attenuation of the visible signal could only result from either scattering by liquid droplets, or by attenuation due to window obscuration from residue and dust buildup. A 35 mm focal length f/1.4 achromatic lens collected the flame luminosity from a broad volume within the combustion chamber and focused it onto a 150 micron diameter multimode silica fiber (50 meter length) directed out of the test cell into the control room where the detector was located. The light emerging from the fiber was directed to an amplified Si photodiode for dynamic luminosity measurements. Calibrated neutral density filters were used to reduce the flame luminosity to levels compatible with the Si photodiode.

The dynamic combustion pressure measurements were obtained using a piezoresistive pressure transducer mounted in a semi-infinite tube arrangement similar to the method used by Darling

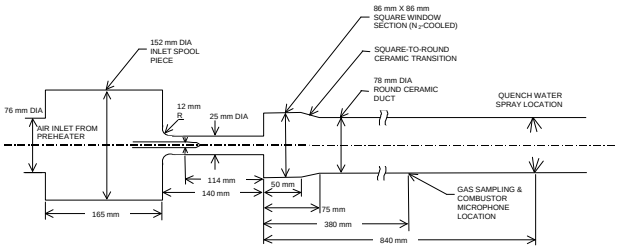

Figure 2: Schematic of LPP combustor rig used in this study. Note that the downstream ceramic lined housing is not shown to scale. The 'Generic' center-body fuel injector is a simple 6.35 mm dia tube with 6 x 0.40 mm radially oriented orifices. Approximately 15% of the total airflow is used for cooling the combustor dome face via backside impingement; the spent cooling air then exits through 16 holes located around the periphery of the dome face (not shown). The quench water spray provides the downstream acoustic boundary condition, while the hard combustor dome face provides the upstream acoustic boundary condition.

et al [29]. The same type of arrangement was used to measure the dynamic pressure in the fuel line immediately upstream of the fuel injector (without the N_2 purge). The dynamic signals from both the infrared absorption, flame luminosity and pressure transducers were low-pass filtered at 12 kHz, recorded and analyzed with a 4-channel dynamic signal analyzer. As most of the acoustic phenomena reside well below 5 kHz, a 12 kHz sampling frequency satisfies the Nyquist criterion while reducing the data storage requirements. Frequency spectrums of the RMS of the dynamic data were acquired by averaging a minimum of 50, 2048-point fast Fourier transforms (FFT) to improve the signal to noise ratio.

The time averaged gaseous emissions produced by the combustor was measured using a retractable, water-cooled, area-averaged extractive sampling probe located 38 cm downstream of the combustor face. The sampling probe is connected to a suite of gas bench analyzers via a temperature regulated electrically heated sample hose. The emissions data was collected and analyzed in accordance with accepted standards for the gaseous emissions testing of stationary gas turbine engines [29]. The measured gases include: NO, NO_2, NO_X, CO, CO_2, HC, O_2 and the measurements were calibrated immediately prior to the experiment against NIST-traceable gas standards.

Figure 2 shows the dimensional outline the premixer and combustion chamber geometry. Note that the downstream ceramic lined combustor housing is not shown to scale. In order to overcome the constraints of proprietary fuel injector designs, a 'generic' LPP fuel injector used in this study. The generic LPP injector was fabricated from a 6.35 mm diameter x 0.89 mm wall thickness stainless steel tube radially drilled at equal intervals with six 0.40 mm diameter orifices. The generic LPP injector had a large measured flow number of approximately 7.0 x 10^{-4} kg s^{-1} $Pa^{-1/2}$ (16.4 lbm hr^{-1} $psi^{-1/2}$) resulting from the lack of a flow constrictor orifice. Flow constriction orifices are sometimes used in fuel injectors to reduce the flow number, and hence the amount of coupling between combustor pressure and fuel injector pressure [30]. This large flow number enabled a larger amount of pressure feedback from the combustion instabilities. Downstream of the injector orifices, a rounded stainless steel nose cone was brazed to the fuel injector tube to reduce flow recirculation, preventing possible flame anchoring behind the injector. The fuel injector was designed as a simple and reproducible source of fuel spray and was by no means optimized or designed for low gaseous emissions operation, but rather to permit the study of acoustic feedback phenomena. The fuel injector nozzle orifices were located 25 mm downstream from the inlet face of a 25 mm diameter premixer tube constructed of a high temperature alloy (Inconel) for heat resistance. The corners of the premixer tube inlet had a 12 mm radius to reduce flow separation inside the premixing tube. The fuel injection orifices were located about 115 mm upstream from the combustor dome face. For the flow conditions inside the premixing tube (typically > 100 m/s), the fuel droplet residence time was typically about 1 ms, preventing auto-ignition effects of the fuel-air mixture inside the premixing tube.

RDG	P_3 (atm)	T_3 (K)	$\Delta P/P_3$ (%)	W_{AIR} (kg/s)	Phi_{METER}	Phi_{RMS}	P_{RMS} (atm)
5900	10.70	759.6	4.034	0.387	0.523	0.417	0.079
5901	10.75	752.7	4.543	0.389	0.587	0.245	0.161
5902	10.39	757.8	4.428	0.389	0.542	0.359	0.099
5903	10.55	753.1	4.303	0.390	0.540	0.368	0.117
5904	10.43	754.5	4.328	0.390	0.516	0.350	0.066
5905	10.24	754.6	4.372	0.389	0.485	0.382	0.076
5906	10.05	761.1	4.598	0.390	0.445	0.306	0.050
5907	16.56	759.9	4.132	0.627	0.513	0.331	0.119
5908	16.47	753.8	4.506	0.631	0.542	0.301	0.228
5909	17.25	751.6	4.290	0.627	0.587	0.159	0.280
5910	16.09	751.3	4.741	0.657	0.484	0.355	0.103
5911	16.71	749.8	4.571	0.637	0.593	0.206	0.316
5912	17.07	757.0	4.351	0.679	0.438	0.367	0.093
5913	16.48	812.4	3.483	0.576	0.518	0.327	0.164
5914	16.54	814.1	3.646	0.565	0.547	0.264	0.200
5915	16.49	815.8	3.869	0.593	0.488	0.345	0.069
5916	16.27	817.4	4.330	0.611	0.440	0.357	0.060
5917	9.97	803.9	5.107	0.394	0.522	0.269	0.055
5918	10.31	806.6	4.596	0.396	0.544	0.316	0.066
5919	9.93	800.8	4.896	0.397	0.487	0.224	0.051
5920	9.94	802.6	4.946	0.392	0.444	0.257	0.044
5921	9.98	700.7	4.141	0.388	0.515	0.381	0.050
5922	10.37	697.3	3.949	0.384	0.580	0.419	0.090
5923	9.99	703.3	4.325	0.396	0.551	0.340	0.059
5924	10.12	702.3	4.820	0.419	0.483	0.371	0.052
5925	13.93	662.8	3.829	0.536	0.562	0.328	0.149
5926	14.19	663.2	4.001	0.533	0.617	0.186	0.227
5927	13.82	667.1	4.921	0.586	0.512	0.367	0.070
5928	13.99	664.5	4.681	0.595	0.483	0.395	0.055
5929	10.20	603.7	4.935	0.435	0.588	0.329	0.167
5930	10.10	605.1	4.852	0.414	0.661	0.245	0.155
5931	9.93	605.6	4.859	0.413	0.633	0.277	0.144
5932	10.20	607.7	5.231	0.444	0.543	0.388	0.108
5933	10.01	604.1	4.877	0.445	0.514	0.385	0.034
5934	5.79	605.5	6.043	0.265	0.590	0.200	0.043
5935	5.64	599.2	5.071	0.230	0.668	0.215	0.054
5936	5.58	603.2	5.317	0.228	0.634	0.234	0.065
5937	5.49	609.6	5.272	0.228	0.550	0.164	0.031
5938	5.39	605.4	5.374	0.231	0.519	0.091	0.023
5950	17.13	754.0	4.590	0.649	0.519	N/A	0.280
5961	10.16	698.0	4.160	0.393	0.593	N/A	0.244

Table 1: Measured combustor settings for all test points used in this study. For each operating condition (grouped by the bold bars), the average of the pressure and temperature are used for the labels of the data presented in the following figures. Also shown on the last two columns are the measured RMS values for the equivalence ratio and combustor pressure. The last two test points were acquired on a separate test with dynamic fuel injector pressures were acquired simultaneously with the combustor pressure and flame luminosity, but without laser absorption measurements.

The combustor dome face was manufactured using a high temperature alloy (Hastelloy-X) and is backside impingement cooled by a fraction of the upstream inlet air flow which then exits around the periphery of the dome face through sixteen 5 mm diameter holes. As an additional measure to reduce the effects of high temperatures on the hardware, the combustor dome face is thermal barrier coated (TBC). With these thermal management practices, the temperature of the combustor dome never exceeded 1000 K, as measured by thermocouple instrumentation on the dome's backside. Furthermore, additional thermocouple instrumentation upstream of the combustor inlet face and on the outside wall of the premixing tube was used to confirm that there was no upstream burning and/or flame anchoring inside the premixing tube. Flame stabilization within the ceramic lined combustion chamber was achieved by inducing a recirculation of the hot combustion products. The sudden expansion of the flow from the 25 mm tube diameter to a 75 mm x 75 mm square cross section introduces a recirculation zone that stabilizes the flame over a variety of operating conditions. However, the efficacy of the sudden expansion stabilization is reduced by the additional air flow along the walls of the combustion chamber introduced by the spent impingement cooling air, and by the N_2 film cooling flow for the windows. These additional flows served to move the combustion

zone downstream and also contributed markedly to the acoustical noise and combustion instabilities of this combustor as evidenced by comparisons with the same combustor operated without both peripheral air and window N_2-film cooling flows. The premixed nature of this combustor arrangement with the film cooling thus suffers from acoustically induced pressure fluctuations at the fundamental longitudinal mode of the combustion chamber (defined by the combustor dome face upstream and the quench water jets located 84 cm downstream). The fundamental acoustic frequency of this combustor ranges from 200-250 Hz and varies with combustion temperature and other conditions. For the purposes of demonstrating the dynamic correlation between acoustic fluctuations and fuel-air ratio fluctuations, this combustor geometry is ideal.

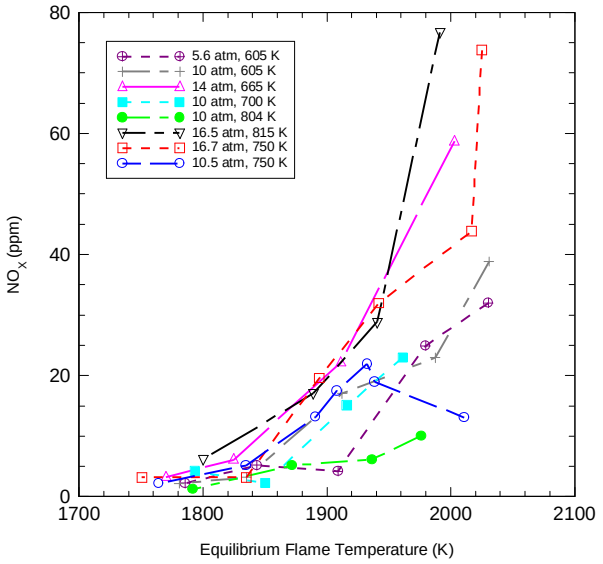

Figure 3: Measured NO_X emissions versus calculated equilibrium flame temperature (at Phi_{METER}) for all data points used in this study.condition.

The combustor was operated with the conditions shown in Table 1. The inlet air pressure, temperature, mass flow rate, pressure drop and fuel equivalence were controlled manually. Operational conditions and gaseous emissions data were monitored and recorded by a facility data acquisition system (16-bit, 1 Hz ADC). Small fluctuations in the operating parameters during the measurement period were averaged over 10 points (10 seconds) and are shown in Table 1. The left column is a serial reading number corresponding to the test point at those conditions. This reading number or RDG will be referred to in subsequent discussions of the data. From Table 1, we can see that the combustor was operated with inlet conditions ranging from 5.5 to 16.7 atm with inlet temperatures ranging from 605 to 817 K at mass flow rates ranging from 0.22 to 0.66 kg/s. The air flow rates were measured using a combination of venturi flow meters and orifice plates with pressure transducers. The fuel flow rates were measured using calibrated turbine flow transducers. All critical measurement data for the facility was calibrated against NIST-traceable standards. The different operating regimes provide a low power 'idle' setting all the way to 'takeoff' full power conditions at high pressure and temperature. Additional test conditions were added to isolate the effect of either temperature or pressure variation with the others held constant.

Results and Discussion:

The generic LPP fuel injector was designed for the purposes of providing a simple source of liquid droplets for the purpose of studying

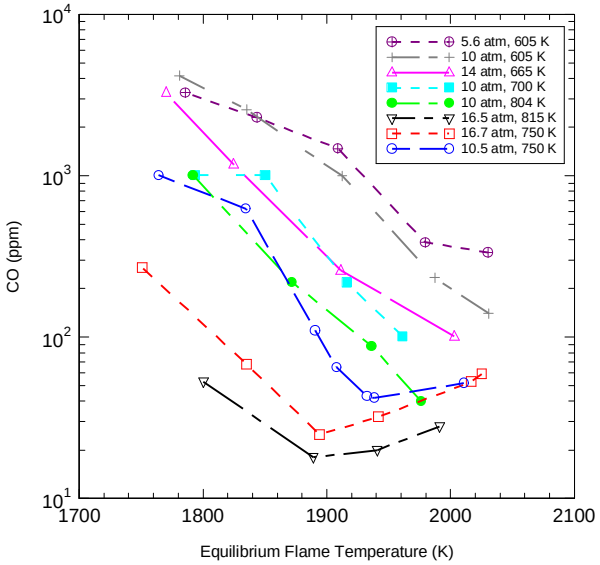

Figure 4: Measured CO emissions versus calculated equilibrium flame temperature for all data points in this study. The broad variation in emissions performance from the 'Generic' LPP injector is indicative of the problems of acoustic coupling and combustion instability that compromises optimum injector performance.

the interaction between equivalence ratio fluctuations and combustion instability. In order to verify that the generic LPP injector behaves in a manner consistent with LP combustion, gaseous emissions measurements of NO_X and CO were measured as a function of metered equivalence ratio (approximately proportional to flame temperature). Figures 3 and 4 show the NO_X and CO, respectively, plotted as a function of calculated adiabatic flame temperature (based on metered equivalence ratios) for all data points listed in Table 1. Note that the data was not customarily plotted versus equivalence ratio calculated from emissions measurements due to the dilution effect of the window N_2 film cooling flow (up to 10% of total air flow). From Figs. 3 and 4, we can see that although the emissions performance of this generic injector is far from ideal, the general behavior of lean LP combustion is exhibited: NO_X levels increase with increasing flame temperature (Phi) and CO increases with decreasing flame temperature (Phi) [31]. The 10.5 atm/750 K curve on Fig. 3 corresponding to RDG 5901 on Table 1 shows the NO_X levels decreasing at the highest equivalence ratio setting. This anomalous behavior is caused by the increased local flame extinction that results from the combustion instability indicated by a high RMS combustor pressure of 0.161 atm or 1.60% of the combustor pressure, P_{COMB} at this setting; Richards and Janus [9] use the (arbitrary) criterion for combustion instability as any RMS pressure value greater than 0.5% P_{COMB}. The increased instability reduces the combustion temperature, thus the NO_X levels also fall correspondingly. This observation is further confirmed by the increased CO emissions at this Phi setting. The rather high levels of CO production in general for this injector would indicate that it has rather poor pre-mixing performance. This injector mixing performance will be determined quantitatively later in this paper by use of the PDF of the equivalence ratio.

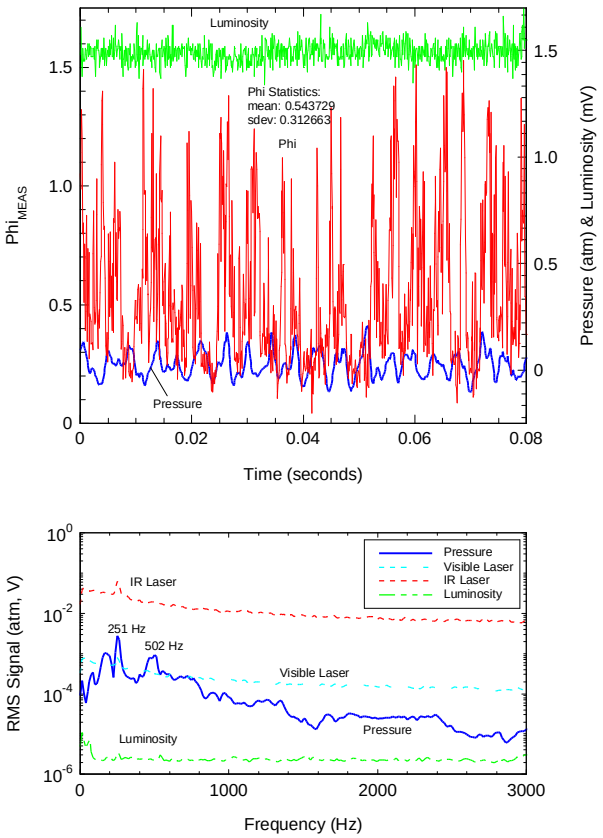

Figure 5: Measured real-time equivalence ratio, pressure and flame luminosity for test RDG 5918 (10.3 atm / 807 K / Phi = 0.544). Note that for this case, the mean optically measured equivalence ratio is equal to the metered equivalence ratio. Lower figure shows the frequency spectrum of the measured variables. Note the acoustic coupling between the IR laser and the combustor pressure at 251 Hz.

Baseline Features in Time and Frequency Space

To demonstrate the real-time nature of the variations in equivalence ratio in a LPP combustor, Fig. 5 shows the optically measured equivalence ratio, the combustor pressure and flame luminosity as a function of time for RDG 5918 (10.3 atm / 807 K / Phi = 0.544). The time span on the abscissa of Fig. 5 is 80 milliseconds. During this period, it is apparent that the equivalence ratio varies widely from about 0.1 to 1.5, but does not show an immediately visible correlation to the pressure fluctuations. The visible flame luminosity does not appear to have any visible peaks or features that one would consider correlated to the pressure fluctuations when viewed by eye. The frequency spectrums of the RMS value of these quantities (shown in the lower graph of Fig. 5) however, tell a different story – there is a definite amount of acoustic coupling between all measured variables at 251 Hz. This frequency compares very favorably to the calculated 253 Hz ¼-wave longitudinal mode frequency of this combustion chamber at the calculated adiabatic flame temperature, corrected for dilution with the metered N_2 film cooling flow. The good agreement between the calculated and measured combustion pressure frequency indicates that it might provide an ideal bulk combustion temperature diagnostic. Although the normalized RMS pressure for this condition (0.67 % of P_{COMB}) is slightly greater than 0.5% as suggested by Richards and Janus [9], it is a relatively quiet condition for this particular injector/combustor combination. Even at this level of acoustic instability, we can see qualitatively from the frequency spectrums that there is a significant amount of acoustic coupling between the fuel injection process and the combustion chamber pressure.

Fig. 5 also shows that the mean of the optically measured equivalence ratio, Phi_{MEAS} matches the metered equivalence ratio, Phi_{METER}. However, the metered equivalence ratio does not indicate that there is a large standard deviation (or RMS of Phi_{MEAS} = 0.31). These measurements show a definite correlation between the fluctuations in the equivalence ratio and the combustor pressure in a LP combustion system at high pressure. Girard et al [20] also found similar evidence of the acoustic coupling between fluctuations in the fuel-air ratio and the combustor pressure at unstable conditions using a laser extractive probe. The quantitative measure of the degree of acoustic coupling will be presented in a separate section.

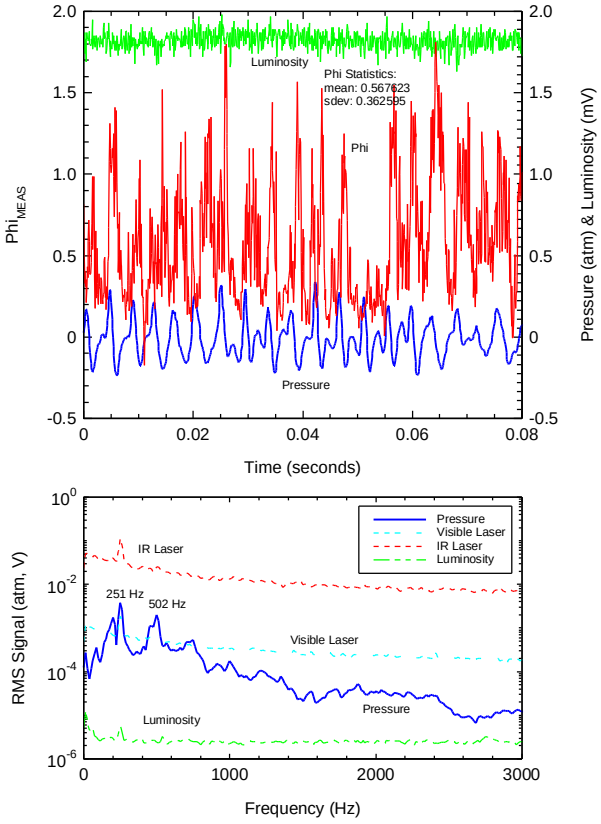

Figure 6: Measured real-time equivalence ratio, pressure and flame luminosity for RDG 5903 (10.5 atm / 753 K / Phi = 0.540). Lower figure shows the frequency spectrum of the measured variables. Note the strong acoustic mode at 251 Hz and its effect of coupling all the measured variables together. The 251 Hz frequency corresponds to the fundamental longitudinal acoustic mode (organ pipe) of the combustor rig.

Inlet Temperature Effects

Figure 6 is similar to Fig. 5 but corresponds to a test point with a slightly cooler inlet air temperature and the same equivalence ratio. This test point corresponds to RDG 5903 in Table 1 (10.5 atm / 753 K / Phi = 0.540). Here the normalized RMS combustor pressure is substantially higher at 1.13% of P_{COMB}, this should translate to a higher degree of acoustic coupling of the combustor pressure into the other measured variables. This enhanced acoustic coupling results from an increased level of combustion instability, which serves to perturb both the rate of fuel flow issuing from the injector and the rate of airflow through the premixing duct. The mean value of the optically measured equivalence ratio (Phi_{MEAS} = 0.57) is a little higher than the metered equivalence ratio (Phi_{METER} = 0.54). This discrepancy is likely due to unburned fuel vapor that is recirculated back into the measurement zone as a result of the increased combustion instability. The combustion instability causes unburned fuel vapor to be recirculated upstream back into the laser probe volume, thereby increasing the effective pathlength of the absorption beam. From the frequency spectrum in Fig. 6, the RMS of the flame

luminosity and the visible laser detector signal can also be seen to increase for this test point. There is a definite acoustic coupling at 251 Hz throughout all measured data channels. In particular, the visible laser channel is substantially higher for this test point than the previous test point due to the reduced amount of fuel vaporization, manifested as an increased liquid phase scattering. The fact that the peak RMS pressure frequency is identical to the previous test point indicates that the bulk combustion temperature for a LP combustor is relatively independent of the change in the inlet air temperature.

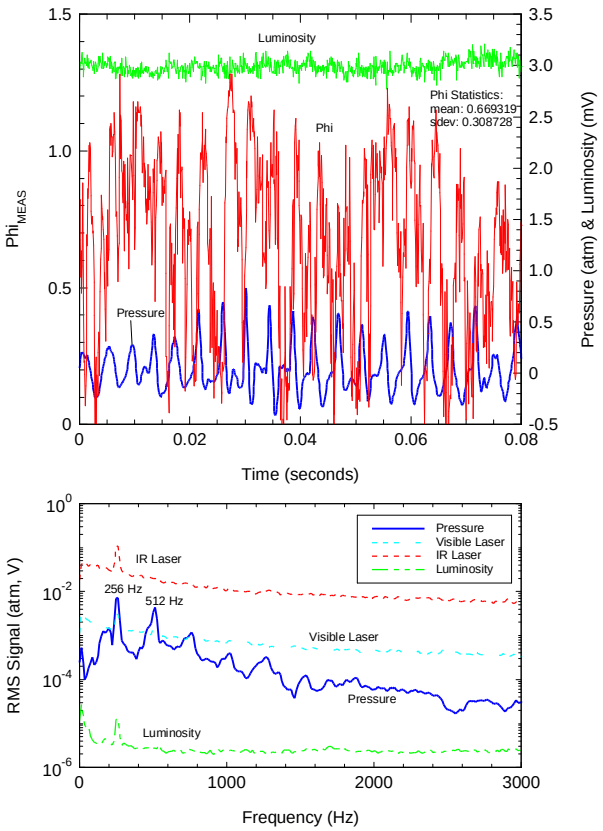

Figure 7: Measured real-time equivalence ratio, pressure and flame luminosity for RDG 5908 (16.5 atm / 754 K / Phi = 0.542). Lower figure shows the frequency spectrum of the measured variables. Note the strong acoustic mode at 256 Hz (frequency is a function of the temperature). The mean of the optically measured equivalence ratio is larger than the metered value due to the increased absorption pathlength during strong acoustically induced flow recirculation.

Elevated Pressure Effects

Figure 7 shows data in the same format as Figs. 5 and 6, but is for a condition with identical inlet air temperature and metered equivalence ratio, but with an elevated pressure. This test point corresponds to RDG 5908 in Table 1 (16.5 atm / 754 K / Phi = 0.542). The upper graph in Fig. 7 shows the temporal variations in the equivalence ratio, flame luminosity and combustor pressure over an 80 ms period. We can see that the equivalence ratio has very large excursions from the mean, sometimes reaching a value of 0 (pure air), we can also see that there are more peak like features in the flame luminosity which appear correlated to the peaks in the combustor pressure. The lower graph in Fig. 7 shows that there is a high degree of acoustic coupling between the IR laser, the visible laser, the flame luminosity and the combustor pressure at 256 Hz. The normalized RMS combustor pressure is 1.38% of P_{COMB} for this test point, which indicates a strong combustion instability according to the 0.5% RMS pressure criterion. Again, the combustion instability causes a large portion of the bulk flow in the combustion chamber to oscillate; this oscillation convects a significant amount of unburned fuel upstream against the combustor dome face which causes the mean of the optically measured equivalence ratio to appear larger than the metered value (Phi = 0.67 vs. 0.54). For this particular case of strong combustion instability, the discrepancy between the average of the optical and metered equivalence ratio is even greater than the previous test point. However, it is not the purpose of this paper to measure absolute equivalence ratios with the infrared laser absorption, but to measure the time-varying equivalence ratio fluctuations. For cases of strong combustion instability such as this test point, the uncertainty in the measured RMS of the equivalence ratio increases due to the change in the effective pathlength resulting from flow recirculation. One way to reduce this effect is to limit the laser probe volume to a region unaffected by the recirculation of the flow fields. This would require placing the measurement probe volume within the premixing duct before the fuel-air mixture enters the combustion chamber. This is would require a complete redesign of the combustor dome to incorporate a fiber optically coupled absorption sensor. This approach is currently under development at NASA Glenn Research Center.

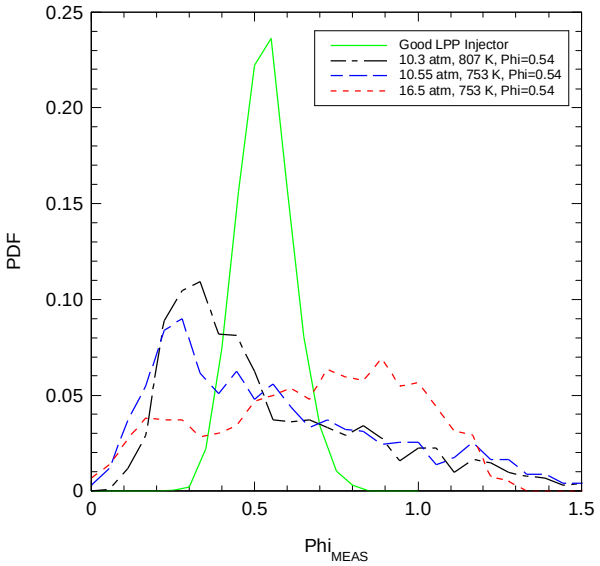

Figure 8: Probability Density Functions (PDF) characterizing the 3 previous time resolved equivalence ratios. A 'Good' LPP injector data obtained from an previous study is shown for illustrative purposes. The Generic LPP injector does not produce the narrow PDF possible with a carefully designed injector.

Equivalence Ratio PDF

As interesting as the time varying equivalence ratio data shown in Figs. 5-7 are, they all kind of look similar after a while. To aid in the comparison of the real time data, the histogram of the equivalence ratio time-series data can be calculated to show characteristics of the fuel injection process for a particular injector and/or flow condition. The normalized histograms of the equivalence ratio represent the PDF of the equivalence ratio for this injector at a particular operating condition. PDF's are often used to model the behavior of scalars in turbulent flows and is a widely adopted approach [32]. To the author's knowledge, the measurement of the PDF of the equivalence ratio in a high pressure LPP combustor at high temperatures and pressures has not been previously demonstrated.

Figure 8 shows the equivalence ratio PDF's corresponding to the three test points shown in Figs. 5-7 plus the PDF from a 'good' fuel injector obtained from an earlier test of a carefully engineered LPP fuel injector design. Note that the width of the PDF of the generic fuel injector is much wider than the good fuel injector. Furthermore, the generic fuel injector may have broad distribution in the equivalence ratio. Whereas, the good fuel injector has a narrow distribution. Figure 8 shows that by plotting the PDF of the

equivalence ratio, the mixing performance of a fuel injector design can be evaluated immediately.

From Fig. 8, we can see that the PDF's for the two 10.5 atm test points have a similar shape with the peak PDF value at about Phi = 0.3, but the high pressure (16.7 atm) test point shows a markedly different behavior in that the peak of the PDF is centered at equivalence ratio of about 0.9. This noticeable change in the shape of the PDF suggests that high levels of combustion instability (RMS P_{COMB} = 1.38%) can broaden the distribution of the equivalence ratio in time. Although the generic fuel injector does produce emissions behavior that is in line with the operation in LP mode of operation, it is by no means capable of providing the best mixing and emissions performance. This can be visualized if one examines the convolution of the PDF with the curves that describe the behavior of the NO_X and CO emissions as a function of equivalence ratio (as shown in Figs. 3-4). Clearly, the generic fuel injector will produce both more NO_X and CO than the good fuel injector for the same operating condition. Simply stated, the generic fuel injector spends more 'time' in equivalence ratio regions that produce more NO_X or CO.

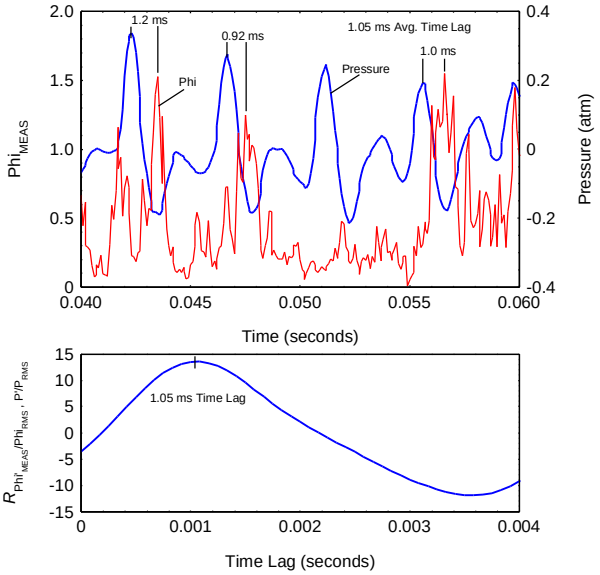

Figure 9: Upper graph shows detail of time series data from Fig. 6 (RDG 5903) showing the time lag between combustor pressure perturbations and measured equivalence ratio perturbations. The time lag corresponds to the advection transport time between the point of fuel injection and laser probe measurement volume. Average time lag obtained from three selected peaks is approximately 1.05 ms. Lower graph shows the cross-correlation coefficient of the equivalence ratio and pressure shown in upper graph as a function of time lag. The first peak of the cross-correlation occurs at 1.05 ms, identical to the value obtained above.

Combustion Instability and Time Lag

In order to examine more closely, the process in which combustor pressure fluctuations affect the fuel injector flow and hence the equivalence ratio, we will re-examine the data presented in Fig. 6 by expanding the abscissa in the upper graph. The upper graph in Fig. 9 shows Phi_{MEAS} and the P_{COMB} over a 20 ms time span from Fig. 6. To demonstrate the concept of the time lag between the pressure perturbation and the equivalence ratio as suggested by Lieuwen and Zin [13], we measure the time lag between three sets of combustor pressure and equivalence ratio peaks from Fig. 7, and take the average. This produces a time lag value of about 1.05 ms. The time lag can also be more accurately determined by taking the cross correlation of the fluctuating component of the normalized equivalence ratio (Phi'_{MEAS}/Phi_{RMS}) and the fluctuating component of the normalized combustor pressure (P'/P_{RMS}) [33, 34]. The resulting cross correlation is a quantitative measure of the degree of coupling between the two

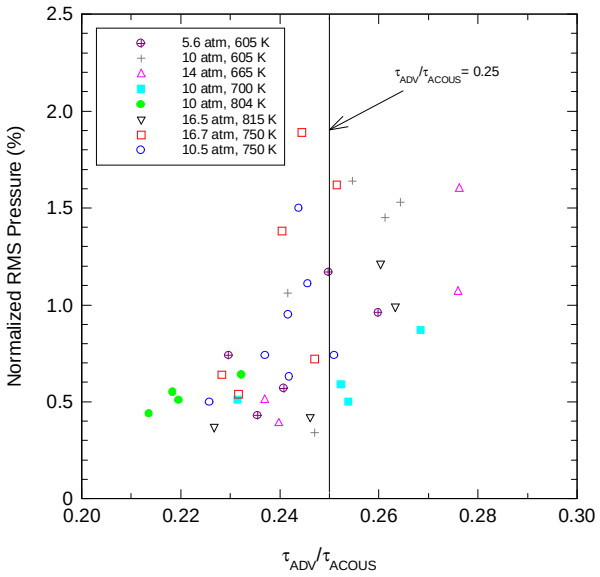

Figure 10: Dependence of combustion instability (Normalized RMS Pressure) with ratio of advection time (τ_{ADV}) to acoustic time (τ_{ACOUS}) scale for all operating conditions. Note that the combustion instabilities increase markedly around τ_{ADV}/τ_{ACOUS} = 0.25 as predicted by Lieuwen and Zin [1998].

terms and is plotted against the time lag. The time lag corresponding to the first peak is the advection time, 1.05 ms which is identical to the approximate method used above.

Combining the advection time with the 116 m/s reference velocity for this test point, yields an advection distance of 121 mm. Further subtracting the 5 mm distance from the combustor exit plane to the laser probe volume, we get a distance of 116 mm which is very close to the 115 mm measured distance between the fuel injection port and the measurement zone shown in Fig. 2. The upper graph in Fig. 9 shows that when there is a sharp, positive pressure perturbation, about 1 ms later, the equivalence ratio increases suddenly. This suggests that pressure perturbations affect the rate of airflow through the premixing duct more than the rate of fuel flow through the fuel injector orifices. Thus, a positive perturbation in the pressure momentarily reduces the airflow, effectively making the mixture more fuel-rich; this shows up after a certain time delay corresponding to the advection time. Using the flow number equation for liquid fuel [30], the measured combustor pressure fluctuations were calculated to have a minimal direct effect on the equivalence ratio; the 0.113 atm RMS combustor pressure for RDG 5903 produces only an approximate 0.01 RMS change in the equivalence ratio based on the measured injector flow number and mean fuel manifold pressure (13.7 atm). This small RMS variation in Phi is almost negligible compared to the measured fluctuations in Phi_{MEAS}. This suggests that the liquid-fueled LPP combustor used in this study operates in a mode similar to a choked-flow gaseous LP combustor, in that downstream pressure perturbations have little or no effect on the direct modulation of the fuel flow. The behavior of choked-flow gaseous LP combustors exhibiting momentary fuel-rich pockets caused by positive pressure perturbations was also suggested by Richards and Janus [9].

Having determined that the time lag of this injector does indeed show up as a measurable change in the time varying equivalence ratio. The combustion instability of this LPP combustor can be examined further using the idea that combustion instability is primarily a function of the mean flow velocity in the duct, and the characteristic frequency of the combustion chamber [9]. Figure 10 shows the level of combustion instability (normalized RMS pressure) as a function of the ratio of the advection time scale (the time lag) versus the acoustical timescale (the inverse of the fundamental frequency). As we can see, Fig. 10 shows that the level of

combustion instability increases markedly around a τ_{ADV}/τ_{ACOUS} value of about 0.25 (indicated by a vertical line). This is in agreement with the analysis of combustion instability in LP combustors performed by Lieuwen and Zin [13]. They predict that zones of combustion instability occur at flow conditions where the ratio $\tau_{ADV}/\tau_{ACOUS} = i - 0.75$ (i = 1, 2, 3, …). For i = 1, this ratio equals 0.25 as observed in this paper. Note that this condition for instability is only valid for combustors with a rigid wall upstream boundary condition (combustor dome face), and a choked-flow fuel injector where the inlet premixing duct is short. This condition is essentially a restatement of the Rayleigh criterion for a specific combustor geometry: when this condition is satisfied, the fluctuations in both the rate of heat release, and the combustor pressure are in-phase, the pressure perturbations in the combustor are thus amplified [10].

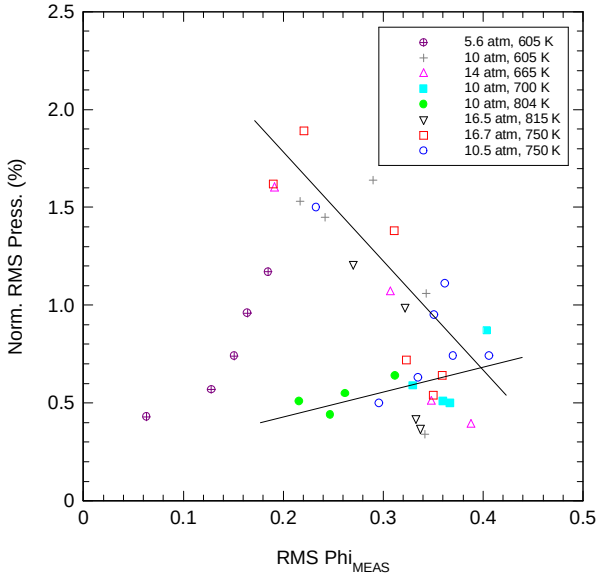

Figure 11: Normalized RMS Pressure fluctuations as a function of RMS equivalence ratio fluctuations for all test points. Lines are added to visually indicate the rough trends. Note that the trends indicated by the guidelines are not monotonic. The 5.6 atm / 605 K data set behaves completely different due to the low temperature and low pressure combination.

Combustion Instability and Equivalence Ratio Fluctuations

After seeing that the level of combustion instability is strongly influenced by the mean flow velocity and the characteristic acoustic frequency of the combustor, we will examine the extent of how much equivalence ratio fluctuations affect the levels of combustion instability. Figure 11 shows the combustion instability level (normalized RMS pressure) as a function of the RMS in the equivalence ratio for all test points. We can see that with the exception of the 5.6 atm data points (crossed-circles) the data all shows two mild trends: as the RMS of the equivalence ratio gets smaller (more uniformly premixed) the level of combustion instability gets larger or sometimes smaller. The non-monotonic behavior of this trend makes it difficult to use as a predictive measure of combustion instability. The trend of increasing combustion instability levels with decreasing RMS Phi$_{MEAS}$ may seem at odds with the notion that perturbations in the rate of heat release (RMS Phi$_{MEAS}$) serve to amplify combustion pressure oscillations. However, recall that homogeneous (perfectly premixed) flows serve as more efficient acoustic amplifiers than heterogeneous flows [30]. Thus, the more well premixed the reactants are in a LP combustor, the more susceptible it is to combustion instability if and only if the rate of heat release and the pressure oscillations are in-phase, as shown in Fig. 10. The 5.6 atm data points in Fig. 11 do not follow this trend because at this condition, the combination of low inlet air temperature (605 K) and low inlet air pressure, cause the injector to produce a poorly atomized fuel spray that remains primarily in the liquid phase as it enters the combustion chamber – causing the combustor to behave more like a conventional non-premixed combustor.

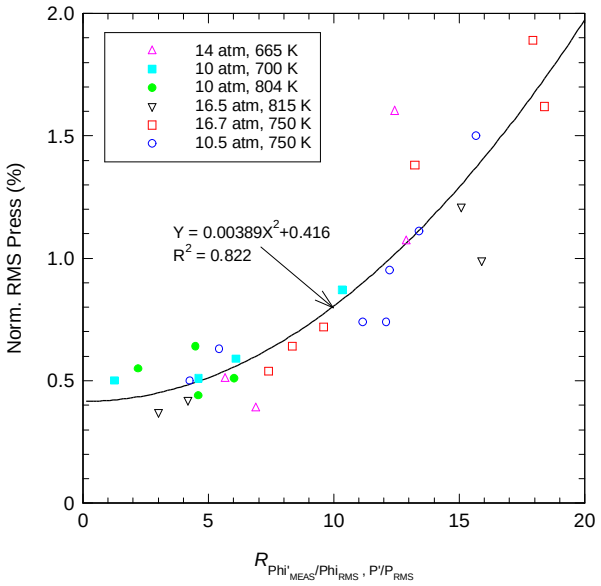

Figure 12: Combustion instability versus the cross-correlation between the fluctuating equivalence ratio and normalized pressure for all data points 655 K and above in temperature. Note that the zero-intercept of the curve fit shows that the level of combustion instability is about 0.4% RMS pressure. This level corresponds to the baseline level of instability inherent in this specific LPP system.

Cross-Correlation of Fluctuations in Equivalence Ratio and Combustor Pressure

Realizing that if fluctuations in the equivalence ratio only contribute to the level of combustion instability when the two quantities are in-phase, we can use the cross-correlation between the two fluctuating components of the normalized equivalence ratio and the normalized combustor pressure, to quantitatively determine the extent of the correlation between the equivalence ratio fluctuations and the dynamic combustor pressure. Figure 12 shows the level of combustion instability (normalized RMS pressure) versus the peak cross-correlation values (at the first peak) for all the higher temperature data points (T ≥ 655 K). The cross correlation value in this case, is a non-dimensional measure of the extent of the coupling between the equivalence ratio and pressure fluctuations. The non-monotonic behavior exhibited in Fig. 11 now is transformed into a single-valued trend. A least-squares fit to the data shows that the data is well approximated (curve fit $R^2 = 0.822$) by a quadratic function. Fig. 12 indicates that the cross-correlation between the fluctuating components of the equivalence ratio and the pressure can be used to predict the level of combustion instability. This observation may prove to be a valuable technique for active combustion control if implemented in real-time using digital signal processing (DSP) circuitry.

Using a laser extractive probe, Girard et al [20] also found that the fuel-air ratio fluctuations in a premixing duct were strongly correlated to the level of combustion instability. Although the technique used by Girard et al [20] introduces perturbations to the flow field due to the sampling probe's 1.7 mm diameter, it has the distinct advantage of being simple to use in that only a small pressure-tight penetration into the premixing duct is required for the extractive probe vs. optical access windows required by the present study. For the purposes of measuring the profiles of unmixedness and its

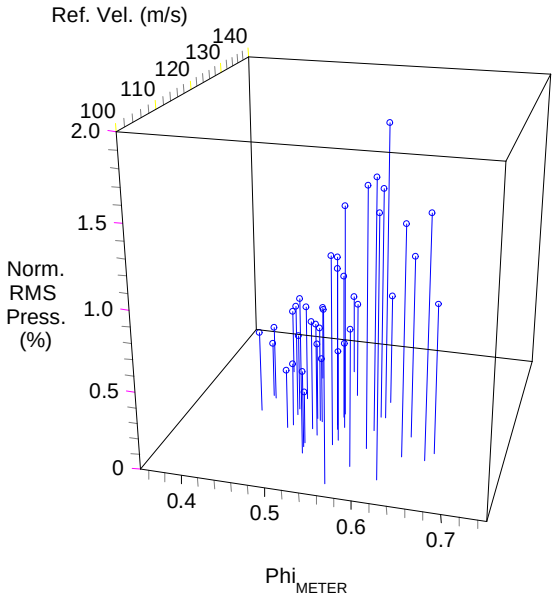

Figure 13: 3-d map of combustion instability (normalized RMS pressure) with respect to the fluctuations in the equivalence ratio (RMS of Phi_{MEAS}) and the reference velocity in the fuel premixing tube for all test points.

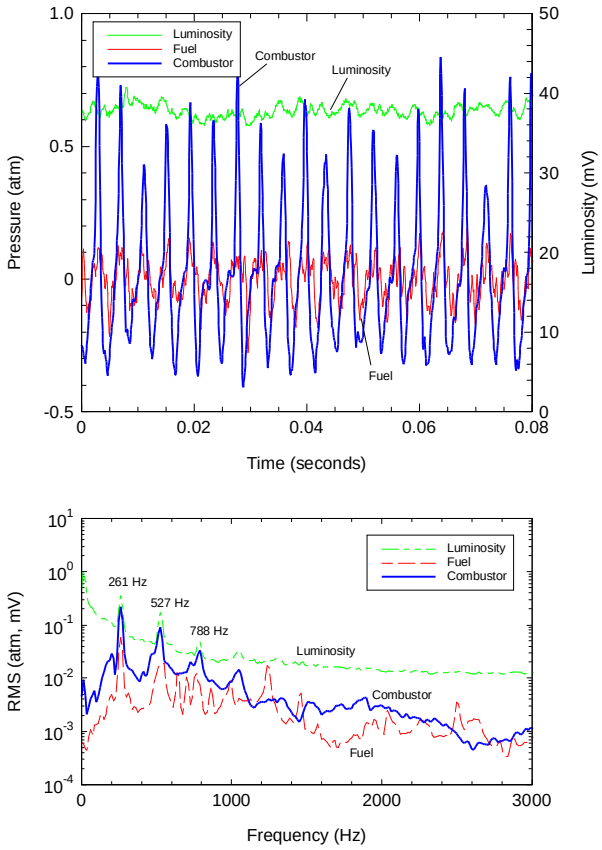

Figure 14: Time resolved pressure fluctuations in combustor and fuel line pressure for test point 5950 (17.1 atm / 754 K / Phi = 0.519). The lower graph shows the clear acoustic coupling between the fuel and combustor pressure evident from the above time resolved traces. Note that the fuel and combustor pressure are in phase whereas the flame luminosity is out of phase.

correlation to combustion instability in a fuel-air premixing duct, the technique employed by Girard et al [20] appears quite satisfactory.

Regions of Combustion Instability

In order to visualize the influence of both the flow velocity and the fluctuations in the equivalence ratio, we can plot a stability plot on 3-dimensional space, in a manner similar to that of Richards and Janus [9]. Figure 13 shows a 'pin plot' (height of the 'pin' corresponds to the ordinate) of the normalized RMS pressure (combustion instability) versus both the reference velocity (time lag) and the RMS of the equivalence ratio fluctuations (perturbations in the rate of heat release) for all test points. Similar to the trends observed by Richards and Janus [9], there is a broad region of combustion instability on this type of 3-d plot. The data shown in Fig. 13 indicate that there is a general region of combustion instability between different inlet temperature and pressure ranges. From Fig. 13, the region of combustion stability appears to be primarily determined by the reference velocity and not by the fluctuations in the equivalence ratio. Moreover, the regions of instability lie in regions where the reference velocity falls below a value of 120 m/s. From Figs. 11 and 13, we can clearly see that combustion instabilities are not determined solely by fluctuations in the equivalence ratio, but also depend strongly on the velocity in the premixing duct.

Fluctuations in Fuel Injector Pressure

For a separate series of tests conducted on another day from the results presented so far, a pressure transducer was fitted onto the fuel manifold to measure the time varying fluctuations in the fuel injector pressure. This additional channel of real time data precluded the simultaneous measurement of the equivalence ratio fluctuations.

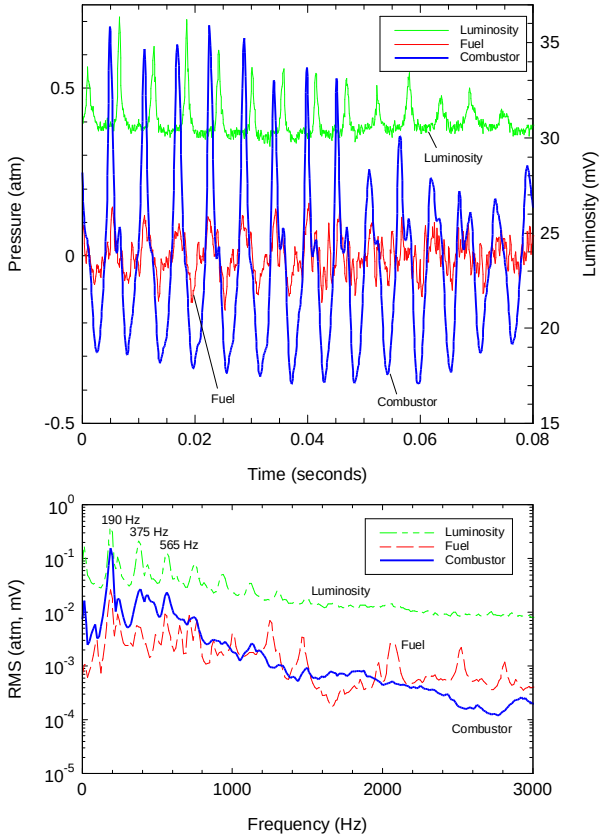

Figure 15: Time resolved traces showing the combustor pressure, fuel injector pressure and flame luminosity for an acoustically noisy test point, number 5961 (10.2 atm / 598 K/ Phi = 0.593). The dynamic combustion pressure amplitude is nearly 1 atm peak-to-peak. The strong coupling of the combustor pressure to the flame luminosity can be seen as evidenced by the pulse like behavior in the flame luminosity.

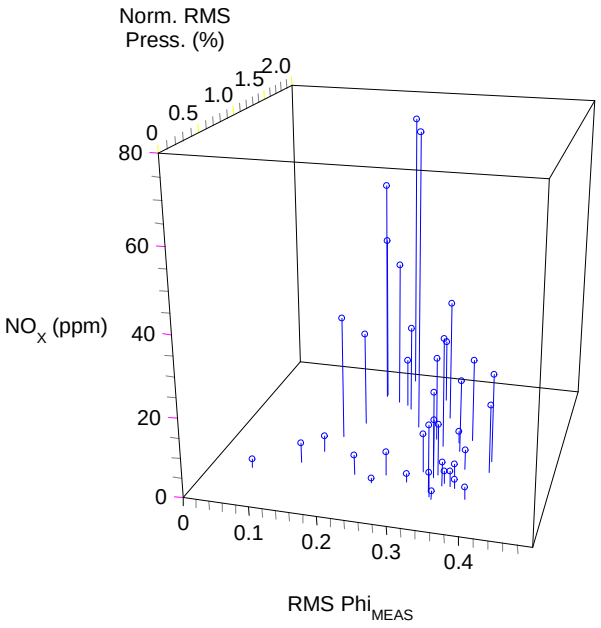

Figure 16: Effect of combustion instability (Norm. RMS Press.) and equivalence ratio fluctuations (RMS Phi$_{MEAS}$) on NO_X emissions for all test points.

Although we have determined that according to the flow number equation for this injector, pressure fluctuations have a minor effect on the direct modulation of the fuel delivery flow rate. Nonetheless, combustion instabilities do arise from very minor perturbations in the rate of heat release, provided that the Rayleigh criterion is satisfied. Figure 14 shows time resolved pressure fluctuations in the combustor, the fuel injector manifold and the flame luminosity for a high pressure condition given by RDG 5950 in Table 1 (17.1 atm / 754 K / Phi = 0.519). On the upper graph in Fig. 14, we can see that pressure in the fuel injector is almost perfectly in-phase with the combustor pressure, owing to the high speed of sound in liquid jet-A and the low restriction in the six fuel injector orifices. The flame luminosity is visibly fluctuating and the peaks appear slightly out of phase with the combustor pressure. The lower graph in Fig. 14 shows that there is a definite correlation between all the measured variables at 261 Hz and its 2nd harmonic at 527 Hz. The high level of acoustic coupling is the result of the large combustion instability (1.71 % RMS of P_{COMB}), which tends to increase the amount of coupling between the two measured variables. Figure 15 shows a test point with an even greater degree of combustion instability (2.51% of P_{COMB}). The top graph in Fig. 15 shows the behavior of the flame luminosity in this dramatic case of combustion instability: the flame luminosity appears to be a pulse-like train in time. The peak-to-peak pressure fluctuations for this test point are approximately 1 atm. The frequency spectrum for this test point shows that the flame luminosity has as many as 7 harmonics of the fundamental frequency at 190 Hz. As expected, for this case we would expect the greatest degree of acoustic coupling between the measured variables at 190 Hz, 375 Hz and 565 Hz.

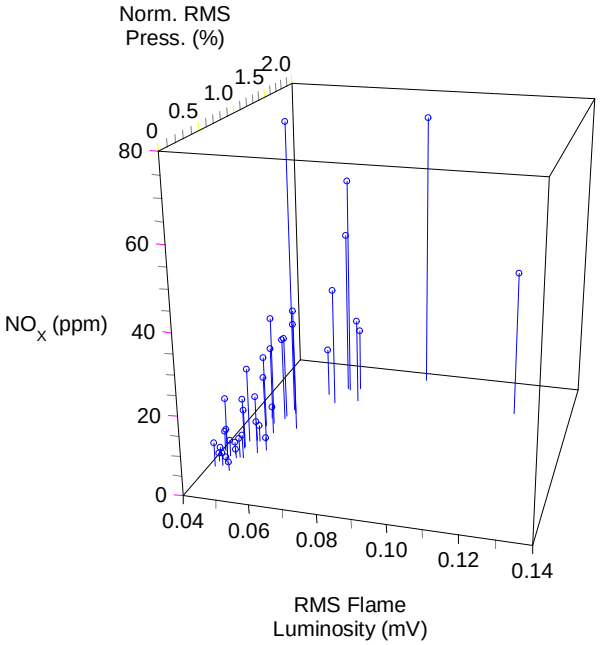

Figure 17: Effect of combustion instability (Norm. RMS Press.) and flame luminosity fluctuations (RMS Flame Luminosity) on NO_X emissions for all test points.

Effect of Combustion Instability on NO_X Emissions

For aircraft engines, the effect of combustion instabilities on gaseous emissions is secondary: an engine must first survive the punishing effects of the large amplitude pressure oscillations from a durability standpoint and the engine must face the imminent threat of flame blowout at altitude. However, assuming these effects are tolerated for minor levels of instabilities (< 0.5% RMS P_{COMB}), it is useful to examine what happens to NO_X emissions when an LPP combustor operates in an unstable regime. Figure 16 shows a 3-dimensional 'pin plot' of the NO_X emissions as a function of both combustion instability and the fluctuations in equivalence ratio for all test points. Clearly, there is a visible trend of higher NO_X with higher levels of combustion instabilities. There is a less obvious trend with respect to fluctuations in the equivalence ratio. As expected, a quiet combustor translates to a cleaner burning combustor. This results from the fact that at high levels of combustion instability, large pockets of non-premixed fuel air are sent into the combustion chamber making the LP combustor operate in a non-premixed mode which has higher

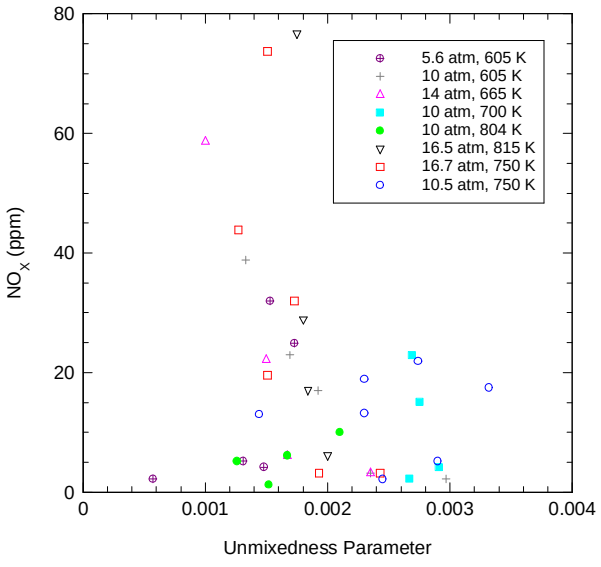

Figure 18: Effect of fuel-air unmixedness on NO_X emissions for all test points. Note that the presence of combustion instabilities is the driving force behind NO_X emissions and for this combustor, precludes the use of the unmixedness parameter to predict NO_X emissions.

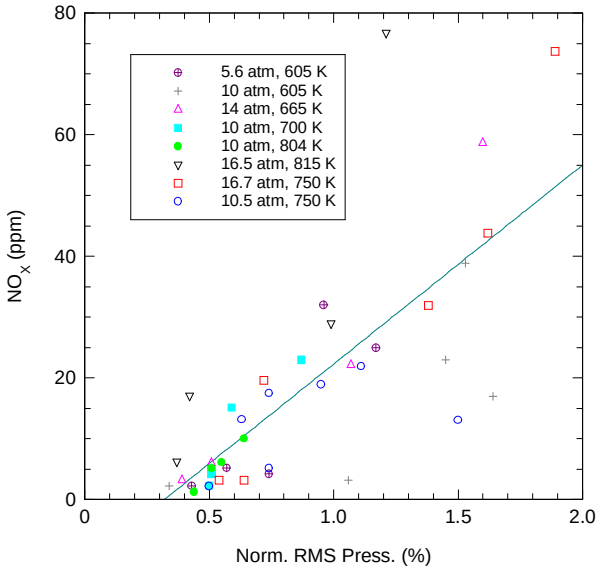

Figure 19: Correlation between NO_X emissions and the level of combustion instability (normalized RMS pressure) for all test points. Solid line is for visual reference and was obtained from a least squares fit to all data. There is considerable scatter, but a trend is clearly evident.

peak combustion temperatures, which generate more NO_X via the thermal NO mechanism. Figure 17 shows a 3-dimensional 'pin plot' of the NO_X emissions as a function of the level of combustion instability and the fluctuations in the flame luminosity for all test points. From Fig. 17, we can see a clear trend of increasing NO_X levels for both the normalized RMS pressure and the RMS flame luminosity. This is observation is interesting in that it indicates that perhaps the simple diagnostic of observing the fluctuating component of the bulk flame luminosity tells us both the level of combustion instability and the level of NO_X emissions from a LP combustor.

If we quantify the level of unmixedness as given Fric [4], and plot NO_X emissions as a function of the unmixedness, we can see

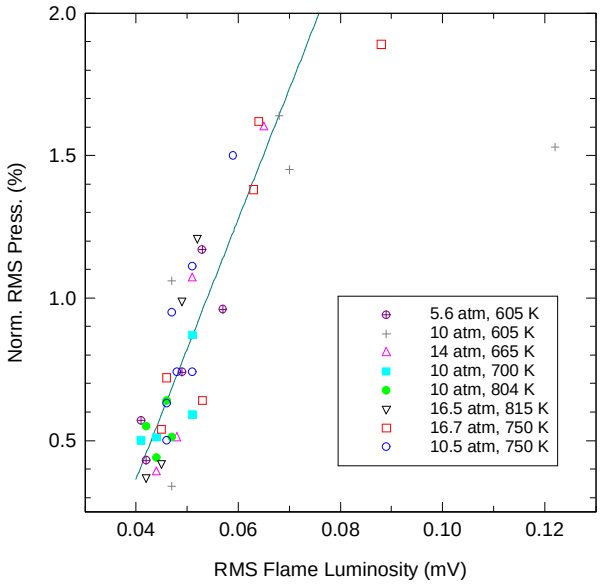

Figure 20: Correlation between level of combustion instability and the RMS of flame luminosity for all test points. Solid line is for visual reference and was obtained from a least squares fit to main cluster of data. Clearly, there is a linear correlation between the two values. This indicates that a fiber optic RMS luminosity sensor may serve as an excellent combustion instability indicator.

that NO_X emissions does not increase with increasing level of unmixedness as predicted by Fric [4]. The fact that NO_X emissions is not purely a function of the unmixedness of the fuel-air ratio (based on the mean and RMS equivalence ratio measurements), is no surprise. When combustion instabilities play a vital role in determining the overall behavior of a LP combustor, the unmixedness alone cannot predict the level of NO_X production. Figure 18 demonstrates this clearly in that there really is no clear trend. However, if we look at the behavior of the NO_X emissions as a function of the level of combustion instability, shown in Fig. 19, we can see that there is a clear trend in the level of NO_X produced a function of the normalized RMS pressure. Although there is some scatter in the data, there is almost a linear correlation in NO_X emissions and normalized RMS pressure. This observation shows the usefulness of monitoring the level of combustion instability in an engine using a simple microphone transducer from the standpoint of monitoring and controlling combustion instability and NO_X. Figure 20 shows the level of combustion instability as a function of the fluctuations in the flame luminosity. Again we can see a clear and almost linear correspondence between the two values. This means that the level of combustion instability is directly proportional to the level of RMS fluctuations in the flame luminosity. This suggests that the use of a simple photodiode to measure the bulk RMS flame luminosity from a combustor (through either a view port or a fiber optic penetration) can be very useful from the same standpoint as measuring the normalized RMS pressure fluctuations, which in turn gives an indication of the level of NO_X emissions.

Conclusions:

Real-time measurements of equivalence ratio, combustor pressure, fuel injector pressure and bulk flame luminosity in a jet-A fueled LPP research combustor were obtained for inlet air pressures and temperatures ranging 5.4 atm to 16.7 atm, and 605 K to 817 K, respectively. In addition, time-averaged gaseous emissions measurements were also obtained using a water cooled extractive probe. In order to provide a database for lean premixed combustion instability model validation, particular attention was given to make the combustor and injector geometry simple and non-proprietary. The complete time resolved data sets for all points shown in Table 1 may be obtained in electronic format for the purposes of modeling combustion instabilities and its effect on gaseous emissions [35].

The real-time equivalence ratio data showed that the instantaneous equivalence ratio can have RMS deviations of order 0.3 to 0.5, even though the time-averaged mean of the measured equivalence ratio matches the metered equivalence ratio. This indicates that there is often a substantial amount of room for improvement in the design of LP fuel injectors even though they may appear to work well from a time-averaged standpoint. In order to compare the performance of a fuel injector at different operating conditions, or to compare different fuel injectors, the PDF's of the equivalence ratios were shown to permit the immediate visualization of the efficacy of different injector designs. By examining the real-time data in both time and frequency space, a large amount of dynamic coupling at the fundamental acoustic frequency (and its harmonics) between all measured variables was also revealed. Of special significance was the finding that the RMS of the bulk flame luminosity was found to track the level of combustion instability in a linear manner. Three-dimensional 'pin plots' of the combustion instability showed that the level of combustion instability exhibited by this combustor was a strong function of the time lag between the point of fuel injection and the combustion zone. This work experimentally confirms that the concept of time lag between the point of fuel injection and combustion as the dominant and perhaps the most controllable aspect of LP/LPP combustor design.

The cross-correlation between the fluctuations in the equivalence ratio and the normalized combustor pressure showed a

strong link with the level of combustion instability. This finding is significant: the above cross-correlation could be used in a real-time manner with DSP circuitry to predict the onset of combustion instability and/or for use in active feedback control systems. The experimental evidence in this paper indicates a mild link between the non-correlated RMS of the equivalence ratio fluctuations and combustion instability, and a strong link between the RMS of the flame luminosity and NO_X emissions with combustion instabilities in a LPP combustor operating at high pressures.

From an emissions stand point, high levels of combustion instability were found to produce high levels of both NO_X and CO emissions, as expected. Somewhat surprising, was the finding that the measured fuel-air unmixedness parameter was *not* found to predict NO_X emissions from this combustor. This is likely due to the fact that the concept of fuel-air unmixedness does not distinguish between stable and unstable combustion. Rather, the level of NO_X emissions from an unstable LPP combustor was found to track both the level of combustion instability and the RMS fluctuations in the bulk flame luminosity.

Acknowledgements:
This research was principally supported by the Ultra Efficient Engine Technology (UEET) Program. The optical instrumentation was provided in part, by the Fast Quiet Engine (FQE) project at NASA GRC. The author is grateful to Mr. A. Turner and Mr. D. Kocan for their assistance in conducting the tests, Mr. Kevin Breisacher for the loan of the dynamic pressure instrumentation equipment, and Dr. Clarence Chang for his insightful comments of the manuscript.

References:

[1] Steele, R. C., Cowell, L. H., Cannon, S. M., and Smith, C. E., 2000, "Passive Control of Combustion Instability in Lean Premixed Combustors," *J. of Engr. for Gas Turbines and Power*," Vol. 122, pp. 412-419.

[2] Correa, S. M., 1992, "A Review of NO_X Formation under Gas-Turbine Combustion Conditions", *Comb. Sci. Tech.*, Vol. 87, pp. 329-362.

[3] Lyons, V. J., 1981, "Fuel/Air Nonuniformity – Effect on Nitric Oxide Emissions," *AIAA Journal*, Vol. 20, No. 5, pp. 660-665.

[4] Fric, T. F., 1993, "Effects of Fuel-Air Unmixedness on NO_X Emissions," *J. of Propulsion and Power*, Vol. 9, No. 5, pp. 708-713.

[5] Nguyen, Q. V., Edgar, B. L., Dibble, R.W., and Gulati, A., 1995, "Experimental and Numerical Comparison of Extractive and In Situ Measurements of Non-Equilibrium Carbon Monoxide in Lean-Premixed Natural Gas Combustion," *Comb. Flame*, Vol. 100, pp. 395-406.

[6] Leonard, G, and Stegmaier, J, 1994, "Development of an Aeroderivative Gas Turbine Dry Low Emission Combustion System," *J. of Engr. for Gas Turbines and Power*, Vol. 116, pp. 542-546.

[7] Anderson, D. N., 1975, "Effects of Equivalence Ratio and Dwell Time on Exhaust Emissions from an Experimental Premixing Prevaporizing Burner," ASME Paper 75-GT-69.

[8] Mularz, E. J., 1979, "Lean, Premixed, Prevaporized Combustion for Aircraft Gas Turbine Engines," NASA TM-79148.

[9] Richards, G. A., and Janus, M. C., 1998, "Characterization of Oscillations During Premix Gas Turbine Combustion," *J. of Engr. for Gas Turbines and Power*, Vol. 120(2), p. 294.

[10] Rayleigh, Lord, J. R. S., 1878. "The Explanation of Certain Acoustical Phenomena," *Royal Institute Proceedings*, Vol. VIII, pp. 536-542.

[11] Bloxsidge, G. J., Dowling, A. P., Hooper, N., and Langhorne, P.J., 1988, "Active Control of Reheat Buzz," *AIAA Journal*, Vol. 26, No. 7, pp. 783-790.

[12] Darling, D., Radhakrishnan, K, and Oyediran, A., 1997, "Combustion Noise at Elevated Pressures in a Liquid-Fueled Premixed Combustor," ASME Paper 97-GT-308.

[13] Lieuwen, T. and Zinn, B. T., 1998, "The Role of Equivalence Ratio Oscillations in Driving Combustion Instabilities in Low NO_X Gas Turbines," 27th Symposium (International) on Combustion/The Combustion Institute, pp. 1809-1816.

[14] Paxson, D. E., 2000, "A Sectored-One-Dimensional Model for Simulating Combustion Instabilites in Premix Combustors," AIAA Paper 2000-0313.

[15] Cohen, J. M., Hibshman, J. R., Proscia, W., Rosfjord, T. J., Wake, B. E., McVey, J. B., Lovett, J., Ondas, M., DeLaat, J., and Breisacher K., 2000, "Experimental Replication of an Aeroengine Combustion Instability," ASME Paper 2000-GT-0093.

[16] Johnson, C. E., Neumeier, Y., Lubarsky, E., Lee, J. Y., Neumaier, M., and Zin, B. T., 2000, "Suppression of Combustion Instabilities in Liquid Fuel Combustor Using a Fast Adaptive Control Algorithm," AIAA Paper 2000-0476.

[17] Sattinger, S. S., Neumeier, Y. Nabi, A., Zin, B., Amos, D. J., and Darling, D. D., 2000, "Sub-Scale Demonstration of the Active Feedback Control of Gas-Turbine Combustion Instabilities," *J. of Engr. for Gas Turbines and Power*, Vol. 122, pp. 262-268.

[18] J.G. Lee and D. A. Santavicca, 1997, "Fiber-Optic Probe for Laser-Induced Fluorescence Measurements of the Fuel-Air Distribution in Gas-Turbine Combustors," *Journal of Propulsion and Power*, Vol. 13, No. 3, pp. 384-387.

[19] Mongia, R. K., Dibble, R. W., and Lovett, J. A., 1998, "Measurement of Air-Fuel Ratio Fluctuations Caused by Combustor Driven Oscillations," ASME Paper 98-GT-304.

[20] Girard, J. W., Dibble, R. W., Arellano, L. O., and Smith, K. O., 2001, "Use of an Extractive Laser Probe for Time-Resolved Mixture Fraction Measurements in a 9 atm Gas Turbine Fuel Injector," ASME Paper 2001-GT-0372.

[21] Nguyen, Q. V., Mongia, R. K., and Dibble, R. W., 1998, "Real-Time Optical Fuel-to-Air Ratio Sensors for Gas Turbine Combustors," SPIE Proceedings, Vol. 3535, pp. 124-130

[22] Tsuboi, T., Inomata, K., Tsunoda, Y., Isobe, A., and Nagaya, K., 1985, "Light Absorption by Hydrocarbon Molecules at 3.392 μm of HeNe Laser," *Japanese Journal of Applied Physics*, Vol. 24., No. 1, pp. 8-13.

[23] Drallmeier, J. A., 1994, "Hydrocarbon-Vapor Measurements in Pulsed Fuel Sprays," *Applied Optics*, Vol. 33, No. 33, pp.7781-7788.

[24] Yoshiyama, S., Hamamoto, Y., Tomita, E., and Minami, K., 1996, "Measurement of Hydrocarbon Fuel Concentration by Means of Infrared Absorption Technique with 3.39 μm He-Ne Laser," *JSAE Review*, Vol. 17., pp. 339-345.

[25] Fuss, S. P., Hall, M. J., and Ezekoye, O. A., 1999, "Band-integrated infrared absorptance of low-molecular-weight paraffin hydrocarbons at high temperatures," *Applied Optics*, Vol. 38, No. 13, pp. 2895-2904.

[26] Bianco, J, 1995, "NASA Lewis Research Center's Combustor Test Facilities and Capabilities," AIAA Paper 95-2681.

[27] Hicks, Y. R., Locke, R. J., Anderson, R. C., Zaller, M., and Schock, H. J., 1997, "Imaging Fluorescent Combustion Species in Gas Turbine Flame Tubes: On Complexities in Real Systems," AIAA Paper 97-2837.

[28] Darling, D., Radakrishnan, K., and Oyediran, A., 1997, "Combustion Noise at Elevated Pressures in a Liquid-Fueled Premixed Combustor," ASME Paper 97-GT-308.

[29] S.A.E., 1982, "Procedure for the Calculation of Basic Emission Parameters for Aircraft Turbine Engines," Society of Automotive Engineering, A.N.S.I./S.A.E. AIR 1533.

[30] Lefebvre, A. H., 1999, Gas Turbine Combustion, 2nd Ed., Edwards Brothers.

[31] Lovett, J. A. and Abuaf, N., 1992, "Emissions And Stability Characteristics Of Flameholders For Lean-Premixed Combustion,", ASME Paper 92-GT-120.
[32] Chen, J. Y., Kollmann, W., Dibble, R. W., 1989, "PDF Modeling of Turbulent Nonpremixed Methane Air Flames," Comb. Sci. Technol., Vol. 98, p.245.
[33] Press, W. H., Flannery, B. P., Teukolsky, S. A., and Vetterling, W. T., 1989, Numerical Recipes (FORTRAN Version), Cambridge University Press, pp.415-416.
[34] Mathcad Professional software, Version 7, Mathsoft Inc, Cambridge, MA.
[35] Request electronic data directly from author via e-mail: Quang-Viet.Nguyen@grc.nasa.gov